

COMPARATIVE ANALYSIS OF TERRESTRIAL AND MARTIAN VOLCANIC  
FEATURES USING MULTISPECTRAL THERMAL INFRARED IMAGES , AERIAL  
PHOTOGRAPHS AND VIKING IMAGES

---

A Senior Honors Thesis  
Presented to  
the Faculty of the Department of Geology and Geophysics  
University of Hawaii at Manoa

---

In Partial Fulfillment  
of the Requirements for the Degree  
Bachelor of Science with Honors

---

by  
**Paraluman Puao'olemauga Stice**

May 7, 1991



Stice, Paraluman Puao'olemauga  
SOEST Library

## TABLE OF CONTENTS

Introduction.....	3
Remote Sensing Data Utilized In This Project.....	6
Viking Mission.....	7
TIMS .....	8
Martian Volcanoes.....	9
Ascraeus Mons .....	10
Olympus Mons .....	11
Tectonics on Mars .....	12
Hawaiian Volcanoes .....	14
Mauna Loa.....	15
The Evolution of Mokuaweoweo.....	16
Observations .....	17
Lava Flows .....	18
Wrinkle Ridges .....	19
Interpretations.....	21
Future Missions	
Mars Observer and Sample Return Mission.....	23
Conclusions.....	24
References Cited.....	26

Thanks to: my thesis advisor and friend, Dr. Peter Mougini-Mark, and to  
Dr. Scott Rowland for all of his help.

**This work is lovingly dedicated to  
Dr. Gary Stice (my favorite geologist) and Apolonia Stice, and  
in memory of Dr. William Coulbourn**

### Introduction

The process of collecting information about an object without physically being in contact with it is often referred to as remote sensing. The utility of remote sensing in fields such as geology, geography, engineering and environmental studies is rapidly increasing with technology. Thirty years ago, being able to study the Earth and other planets through remote sensing was merely a dream. We were already realizing the benefits of utilizing air photography in solving scientific problems. We began obtaining information from images beyond the visible portion of the electromagnetic spectrum. Today, we are able to sense data from space and conduct global, uniform studies on planetary bodies. For the geologist, the field of remote sensing opens up a whole new level of interpretation. Inaccessible areas of the Earth and other planetary bodies can now be studied uniformly with increasing detail.

In studying planetary bodies, remote sensing is currently the best option. The field of "planetary geology", geology applied to other planets and bodies, is growing rapidly as technology increases our ability to obtain information about other planets. We have built up our knowledge of the solar system, beginning with the early telescopes of Galileo and on to advanced radiotelescopes. Optical telescopes are still very useful for obtaining data from the Moon, which is relatively close to the Earth. However, in some applications, earth-based observations in geology have been nearly exhausted, or planets further away or those obscured in any way, we must rely spacecraft images, which offer up to 1000 times better resolution (Siegal and Gillespie, 1980) in the case for Mars.

Of the solar system's nine planets, the four inner planets, Mercury, Venus, Earth and Mars, are considered terrestrial planets. They are characterized by rocky surfaces, as opposed to the Jovian planets, which are most likely gaseous balls composed primarily of

hydrogen, helium, and other light elements (Carr, 1984). By studying the geologic processes involved within the Earth, we have developed many theories about the evolution of the Earth's surface and the planet's history. By way of analog, geologists must therefore examine key characteristics in surface morphology of other terrestrial planets in an effort to further understand their interrelationships.

Mars is approximately 0.51 times the size of Earth in diameter and 1.88 times that of the Moon. It has a mass of about  $6.418 \times 10^{26}$  g (Arvidson et al., 1980) and is less dense than the Earth. Mars has been extensively studied with spacecraft exploration beginning with the Mariner 4 flyby in 1965 and continuing with Viking Missions, which collected data until 1981. Since the discovery of volcanoes on Mars, there has been a strong case for comparative studies of the Earth and Martian shield volcanoes. Attempts at understanding the enormous volcanoes found on the surface of Mars have been based on what we know about volcanic processes which occur on the Earth. In Hawaii, where the classic shield volcanoes of the Big Island offer relatively accessible and well documented histories, the geology by analog method has been particularly useful. Volcanic features common on shield volcanoes such as lava channels, collapsed lava tubes, levees and flow fronts have been compared to similar features found on Mars. The summit areas of Martian volcanoes have simple to complex calderas, most of which have Earth analogs.

As we learn more about Mars, revisions have been made to the notion of using Hawaiian shields as direct analogs. Mouginis-Mark (1981) noted that one needs to consider more evolved terrestrial volcanoes such as those found in Galapagos, Reunion and Iceland. Greeley (1980) cautioned against not considering other volcanic regions, noting that terraces on flanks are dominant features on Martian volcanoes, but are not as readily found in Hawaii as they are in the Galapagos. Crumpler and Aubele (1978) have also cited Galapagos volcanoes as more appropriate analogs. In another paper (1989)

Crumpler and Aubele categorized the Martian volcanoes into four categories, each with different Earth analogs.

During the course of this thesis research, I studied many forms of remotely sensed data. The goal of my first semester was to learn about remote sensing and Mars volcanism, both relatively new subjects for me. For the actual project, I narrowed the study to examining three types of data: color air photographs, black and white Viking images, and Thermal Infrared Multispectral Scanner (TIMS) images. In studying volcanic provinces, I noticed there was an advantage to using color air photographs over black and white images, and that advantage was far greater when supplemented with TIMS data. The resolution and quality of the data available for Mauna Loa made it difficult to draw parallels with the Martian volcanoes based on Viking images, which are black and white and of poorer resolution. This was particularly true when comparing features such as volcanic flows which require detailed data on contacts. It was difficult to quantify with confidence length, source and nature of flow units using Viking images.

In preparation for future Mars Observer Missions and sample return precursor missions, data such as this will prove to be extremely useful in mapping the surface, and in defining similarities of Martian and terrestrial volcanoes. Many features which are not obvious on black and white or may be difficult to distinguish, even in color, are distinguishable in TIMS scenes. Applying a combination of data sets makes it easier to perform volcanic studies, especially for examining occurrences of features such as flank lava flows or other structural information. This study will therefore compare color air photos and TIMS images for Mauna Loa, with Viking images of Mars, in an effort to assess their value in planetary studies of volcanoes. The Earth-Mars analog will be utilized here, emphasizing the application to volcanic provinces, namely the flows near or on the caldera rim and the intra-caldera tectonic features. On Mars, I have chosen to study the

summits of Olympus Mons and Ascraeus Mons, where high resolution images are available of the summit areas, in comparison with Mokuaweoweo Caldera of Mauna Loa, for which we have air photographs as well as TIMS images.

As the study progressed, I found that there were two very prominent features of the three volcanoes which warranted careful observation: the nature of wrinkle ridges on the caldera floor and the presence of flank eruptions for all three of the volcanoes studied. I felt that within the scope of this project, examining and comparing these two features would be the most useful.

#### Remote Sensing Data Utilized In This Project

The three types of remote sensing chosen for this project (Viking images, air photos and TIMS images) are each acquired separately, and must be viewed with different techniques. For example, in looking at Viking images, one needs to bear in mind the direction of the sun angle relative to the image. This gives the sense of positive and negative relief, which is easily misinterpreted. One must also be careful not to assume too much in quantifying relative relief, which is most reliable when obtained through photoclinometric data. The air photos were obtained from the same aircraft as the TIMS data, on the same day. In viewing air photos, one must again consider sun angle, angle of the aircraft, and height of aircraft. TIMS data can be extremely complex, especially in viewing either a principal component or decorrelation stretch. Therefore, for this study, analysis was not aimed necessarily at extracting quantitative data from each different color viewed in a scene. Rather, color differences were interpreted as distinct contacts which indicate a transition in the nature of the surface. Brief background information on the Viking Mission and TIMS data follow.



## Viking Mission

The Viking Mission was a project which evolved out of the Mariner Mission of the 1960's. The Mariner 4 returned pictures with a resolution of one kilometer, about 150 times better than earth-based observations. By Mariner 9 in 1971, the resolution was down to 100 meters. Mariner 9 obtained 7300 images of Mars and was the first spacecraft to go into orbit around another planet (NASA SP-441)

Viking Orbiter 1 was launched on August 20, 1975 and arrived at Mars on June 19, 1976. It performed a flyby of Phobos, Mars' larger inner moon. Viking Orbiter 2 arrived at Mars on August 7, 1976. Viking 2 was able to observe the polar regions at relatively close range. It flew by Deimos, another of Mars' moons. Both Viking Missions consisted of an orbiter and a lander (figures 1 and 2), plus other scientific instruments. Viking 1 landed on the planet on July 20, 1976 in Chryse Planitia. On September 3, Viking 2 landed on Utopia Planitia. Since one of the goals of Viking was to detect if life on Mars was possible, chemical and meteorologic conditions near the landing site were measured.

The cameras used to obtain Viking photographs were two slow-scan vidicons mounted side by side on the orbiter. A faceplate on the vidicon was induced by light of varying intensity. The light was read by scanning the plate with an electron beam (Carr, 1981). The current was digitized to 1182 x 1056 pixel pictures. The data were relayed back to Earth with a travel time of approximately 20 minutes.

Data were processed at JPL in Pasadena. First, they were compiled to video format, then corrected for noisy data or missing transmissions. This was done by filling the space in with the average value of adjacent pixels. A filtered and shaded version of each frame was produced. The shaded version was made to emphasize contrast where the scene was narrow. The filtered version was also produced to emphasize topographic detail, useful in areas where large albedo variation or contrasts in illumination occurred.

## TIMS

The Thermal Infrared Multispectral Scanner (TIMS) is a NASA airborne instrument. TIMS data have been used to obtain relative dates of lava flows in mapping and to assess chemical and physical properties of a surface (Kahle, et al., 1988 and Abrams et al., 1991). The multi-spectral scanner utilizes electronic energy detectors to sense energy in a number of different narrow spectral bands. One advantage of multi-spectral data is that the same optical system is used to collect data in all spectral bands simultaneously (Lillesand and Kiefer, 1987). Further, image enhancement techniques such as decorrelation stretches and principal component stretches can be performed on data, which are easily calibrated and transmitted due to their electronic nature (Figure 3). TIMS operates in the thermal infrared portion of the electromagnetic spectrum. It has six bands, between 8.2 and 12.2  $\mu\text{m}$ , and a total field of view of 80°. Images are obtained using a mirror which scans  $\pm 38^\circ$  about nadir, perpendicular to the line of flight. The data set we looked at was obtained over the island of Hawaii in November of 1985 on NASA's C-130 aircraft. The instrument was flown 7.7 km above sea level with a nadir ground resolution of 25 m/pixel. There were 64 flight lines over Kilauea and Mauna Loa. Infrared data were also obtained simultaneously (Kahle et al., 1988). The radiance of a surface is a function of the temperature and spectral emittance, and since emittance is related to composition, this is the more important information contained in the data. A decorrelation stretch was performed on the data to emphasize the emittance instead of the temperature.

The characteristic spectral differences of the lavas of varying ages have been established by Kahle and others (1988). They found that pahoehoe and a'a flows are consistently separable by a pronounced color change with age, even though the lavas are compositionally identical. The color difference on the TIMS image was due to weathering

of the surface, suggesting an age difference. Other effects visible in TIMS data were physical and chemical degradation of glassy crusts, accretion of silica-rich coats, replacement of basalt by iron oxides, and vegetation. When analyzed in conjunction with other data such as the visible/near-infrared/short-wave infrared (VNIR) images (Abrams et al., 1991), results can be even more conclusive.

### Martian Volcanoes

Before Mariner 9 images were obtained of the surface of Mars, earlier Mariner mission data were generally interpreted based on what we knew of the Moon. Hence, volcanic provinces of Mars were originally thought to be similar to the heavily cratered terrain of the lunar highlands (Mutch et al., 1976). During the Mariner 9 mission, scientists cited four black spots on the surface. By directing narrow-angle cameras at the spots, it was revealed that they each had a caldera-like depressions at the top. Hence, the planet was not as inactive as originally believed.

There are three main volcanic provinces on Mars: Tharsis, Elysium and Hellas. Contained within the Tharsis region (centered at 0° and 115°W) is the Tharsis bulge, the most elevated region on Mars, and four large volcanoes (Figure 4). Three of the volcanoes lie along a 700 km line trending northwest and are referred to as the Tharsis Montes. They are, from the southwest, Arsia Mons, Pavonis Mons, and Ascraeus Mons. Olympus Mons, the largest volcano on the planet and in the solar system, is located 1600 km northwest of the line. Also located in the region are smaller volcanoes Biblis Patera, Ulysses Patera, Jovis Tholus, Uranus Patera, Ceraunius Tholus, Uranus Patera and Tharsis Tholus. The Elysium region (25°N, 210°W) contains three volcanoes: Albor Tholus, Hecates Tholus, and Elysium Mons. The Hellas region (40°S, 290°W) contains the older volcanoes Hadriaca Patera, Amphitrites Patera, Tyrrhena Patera, and Apollinaris

Patera. The oldest volcanoes such as Hadriaca, Apollinaris and Amphitrites Paterae are disparate in location and generally have less vertical relief. The younger and larger volcanoes occur in the Tharsis and Elysium provinces (Carr, 1981).

The Tharsis Montes are similar in diameter (350-400 km) and height (24-27 km). The flanks slope at around 5 degrees (Blasius, 1979) and exhibit surfaces with lava channels and long narrow flows (Carr, 1981). Each summit contains a caldera, although they are different in diameter, ranging from 110 km (Arsia Mons) to 40 km (Ascraeus Mons). Comparable in geometry to Hawaiian shield volcanoes, the three Tharsis Montes have similar growth cycles. The shield-building stage formed the main shield through eruption of fluid lava from fissures and the summit. Since the volcanoes are fairly symmetrical and there are not any obvious rifts, it appears that most of the lava was probably erupted from the summit of the volcano. After caldera collapse, lava was transported laterally to the flanks, where numerous eruptions created volcanic plains.

#### Ascraeus Mons

Ascraeus Mons is the northernmost of the Tharsis Montes (Figure 5). Located at 11°N, 104°W, it is approximately 300 km in diameter and rises about 17 km above the Mars datum. The summit has a multiple caldera formed by several collapse events. Mouginis-Mark (1981) delineated eight collapse features at the summit, and devised a relative chronology based on cross-cutting relationships. In center of the caldera, the largest (40 km diameter) crater appears to have formed last, with intermediate (20-30 km) and smaller (7-15 km) craters forming earlier. The lack of source vents for lava flows on the southern edge of the caldera suggest that each subsequent flow was truncated by the various collapse events (Crumpler and Aubele, 1978). Lack of slump blocks on each crater floor of varying depths further suggests that after the formation of each crater, the caldera

floor was resurfaced (Mouginis-Mark, 1981). Crater counts for two frames (90A49 and 90A50) show low distribution of craters on the southeast, indicative of recent obliteration of small craters.

There are fewer arcuate grabens on Ascraeus Mons than on the other two Tharsis Montes. However, concentric crater-chains are fairly common, found between 40 to 120 km from the summit. In the northeast and southwest, grabens are aligned with crater chains oblique to the concentric crater-chains. These crater chains of the northeast and southwest flanks are similar to those on the other volcanoes, except that on Ascraeus Mons they have developed into complex tributary-like networks, which suggest that the clusters may be the source of lava flows. The arcuate grabens may be another source of lava (Crumpler and Aubele, 1978).

### Olympus Mons

Olympus Mons (Figure 6) has a summit 27 km above the Mars datum and is 700 km in diameter. It also has a nested caldera (80 km) made up of six craters (Mouginis-Mark, 1981). An aureole surrounds the base of the volcano about 300-700 km away from the escarpment. On Olympus Mons, superposition indicates that the largest (66 km) crater formed first, with later events producing small and intermediate sized craters around the rim. Unlike Ascraeus Mons, Olympus Mons does not appear to have any lava flows on the caldera floor, and very few appear on the flanks. The floor fractures are wider at the caldera rim and narrower toward the center, which indicates a tectonic feature possibly related to the solidification of the lava lake or the lack of support from the underlying magma chamber. The mechanism for the floor fractures do not appear to have had an effect on the existing crater walls, so it is unlikely that they are structurally related. A landslide appears on the southern end of the rim, with material extending about 2 km onto the caldera

floor. This may be a result of an impact event or of the greater susceptibility of the walls of Olympus Mons.

### Tectonics on Mars

Tectonics on the Earth is dominated by the effects of relative plate motion. The movement of plates of lithosphere over the asthenosphere affects virtually all geologic processes, including volcanism. The constant motion of plates and subsequent subduction at trenches and extrusion at ridges makes the Earth very dynamic, with most of the seafloor younger than Jurassic in age (Cox and Hart, 1986). In contrast, Mars has a fixed crust and is essentially void of tectonic features such as mountain belts and subduction zones. The lithosphere does not appear to have been recycled as it is on Earth. The large features on Mars, despite its size, is a result of the inability of the planet to achieve equilibrium through hydrologic or other processes (Carr, 1981).

On Mars, Ascraeus Mons has been described as having a stronger influence of regional stress than Olympus Mons by Crumpler and Aubele (1989). This is seen in a linear pattern of one well-developed orientation. A single fissure trend usually cuts through the central caldera. There is also a concentric arrangement of faults and fissures near the summit. Olympus Mons is described as being more similar to Hawaiian type volcanoes, with the flank structure having moderate influence and interaction with regional stress fields. This influence is seen in the tendency for rifts, vents and fissures to follow pre-existing structural fabric orientations as well as regional stress orientations. Hence the volcano reflects tectonic and body stresses.

It has been found (Thomas et al., 1989) that the escarpments of Olympus Mons are thrust faults resulting from compression of a full magma chamber, and that the terraces of Ascraeus Mons are also likely of the same nature. These thrust faults formed

penecontemporaneously with the flows and are a result of compressional failure of the cone. Similar faults are also found on Arsia Mons and Pavonis Mons, the other Tharsis Montes.

Wrinkle ridges, often called mare ridges due to their similarity to features found on the moon, are also seen on Mars. In fact, Mars has the greatest distribution of wrinkle ridges observed on a terrestrial planet (Watters, 1988). On Mars, they are seen in smooth plains material within a variety of locations throughout the planet in basins (Schiaparelli, Huygens and Copernicus), lowlands (Chryse and Amazonis), plains units (Syrtis Major, Hesperia Planum, and Malea Planum), the Tharsis Plateau, and within calderas (Olympus Mons and Ascraeus Mons) (Basaltic Volcanism Study Project (BVSP, 1981)). Martian ridges are almost indistinguishable in morphology from their lunar analogs (Watters, 1981).

The origin of wrinkle ridges on terrestrial planets has long been debated. In summary, three main hypothesis exist: 1) that they are due to the extrusion of lava along major fractures, forming dikes, sills or laccolithic-type near-surface intrusions; 2) they are formed when lava sheets are draped over buried highland or other structural ridges following subsidence; and 3) they are produced by compressional forces due to loading of the lithosphere by the lava flows. It is generally agreed up on, however, that the ridged plains materials on Mars are the result of flood volcanism (Mouginis-Mark et al., 1981; BVSP, 1981), apparently where lava flows were thick (Lucchita and Klockenbrink, 1981). A volcanic origin for ridges is suggested by association with apparent lava plains and development inside calderas. Further, the morphology of the ridges supports the view that they are compressional features. The Columbia River Plateau near Yakima, Washington has been suggested by Greeley and Spudis (1978) as a terrestrial analog for the plains ridges of the Moon. They are unique in that they developed within thick units of rock with

massive beds, are of recent age, and they developed without overburden, under stresses near the surface (Lucchita and Klockenbrink, 1981).

### Hawaiian Volcanoes

The volcanoes of Mars literally dwarf their Earth counterparts. Olympus Mons is about three times higher than Mauna Loa, the largest volcano on Earth. This is probably due to a thicker and more stable lithosphere on Mars (Carr, 1981) and the absence of plate tectonics. Hawaii is part of the Hawaiian-Emperor volcanic chain, approximately 6000 km long, and consisting of at least 107 individual volcanoes. The Hawaiian Islands lie at the southeast end of the chain, and are considered to be the youngest.

Plate tectonics plays an active role in the formation of many intraplate volcanoes. The hot spot theory best explains the mechanics behind the formation of the Hawaiian Islands, and the Hawaiian-Emperor chain. In the Pacific Basin, we see aligned islands which indicate the direction of plate movement at the time the islands were formed. Presently, the Pacific plate appears to be moving in a northwest-southeast trend. As the plate moves over some sort of melting spot in the mantle, termed a hot-spot. Volcanoes formed from hot-spots make up less than one percent of world's total volcanic activity (Macdonald et al., 1983).

The islands which make up the state of Hawaii and island northwest of the state comprise the Hawaiian Chain. The prevalent style of volcanism in Hawaii is the Hawaiian style. Lava is usually extruded as fire fountains from 5 m to over 500 m. Only a very small amount of the lava cools quickly to become pyroclastic deposits; most of it flows away (Walker, 1990). Also represented in Hawaii are the Strombolian style eruptions characteristic of rejuvenations stage eruptions (Mauna Kea, Haleakala). Surtseyan style eruptions occurs when large amount so water comes in contact with the vent, creating base



surges (Koko fissure, Salt Lake). The youngest member of the Hawaiian Chain is the submarine volcano Loihi, which is estimated to emerge as an island within the next several thousand years.

The Big Island of Hawaii (Figure 7) consists of five volcanoes, three of which have been active in historic time. They are Kohala, Hualalai, Mauna Loa, Mauna Kea, and Kilauea. The older volcanoes are often considered to be Hualalai, Mauna Kea and Kohala. The summits of these volcanoes have cinder and spatter cones. Younger flows cover any evidence of calderas, if they were present at any time. Hualalai and Mauna Kea are considered to be in the alkalic cap stage, as they move off the hotspot. Hualalai has had one historic eruption in 1800. Kohala, the oldest volcano on the island, last erupted about 60,000 years ago and is considered extinct (Walker, 1990). Kilauea and Mauna Loa have been active in historic time.

#### Mauna Loa

Mauna Loa is probably made up of two huge shield volcanoes that mostly erupted tholeiitic basalts, olivine basalts and oceanites (Macdonald et al., 1983). The rocks, all of Pleistocene age (Stearns, 1985), associated with Mauna Loa are the Ninole Volcanics, overlain by Kahuku Volcanics, Pahala ash and Ka'u volcanics. It is estimated that Mauna Loa took approximately 0.5 million years to form. About 40% of the surface is younger than 1000 years old (Lockwood and Lipman, 1987), with declines in output in 1868 and again in 1950. All historic (since 1832) eruptions are of the Ka'u series.

There are two major rift zones on Mauna Loa, one trending southwest and one northeast. Mokuaweoweo, summit caldera of Mauna Kea (Figure 8), is 5 km long and 3 km wide. It resulted from collapse and is growing broader in a northeast-southwest trend. It is a fairly young structure, truncating flows only 590 years old (Lockwood and Lipman,

1987). The western cliff of the caldera rim is 180 meters, as compared to the eastern rim, which is only 70 meters. The caldera was first mapped by Wilkes in 1841. At the time, it had a circular central pit and benches on both sides. North Bay was a separate pit crater. Since 1841, three pit craters have coalesced to the caldera along the original northeast-southwest trend. Eruptions are usually of two types: summit eruptions contained within Mokuaweoweo or flank eruptions which begin at the summit and are subsequently erupted at the lower altitudes either continuously along a fissure or by breaking out lower down along a new one (Lockwood and Lipman, 1987). In historic time the caldera has absorbed about 30% of the volcano's output (Walker, 1990). The highest frequency of activity in historic times has been at the summit, where most historical eruptions began with activity within the caldera.

Most vents of Mauna Loa are the high-fountaining type, which generally yield a'a flows. Pahoehoe flows are obtained as derivatives of a'a flows or are erupted as volatile-poor lavas. The two types of lava weather differently, making it difficult to obtain age relations, particularly in older terrains. Although the relative distribution of a'a and pahoehoe is about equal,, they vary greatly for flows derived from rift and summit areas. On rift zones, a'a is more likely to be erupted from high fountains. Where slopes of the volcano are steeper, as in the SWRZ, the a'a is also more abundant. Pahoehoe is generally found in the summit areas where lava lakes persisted before the caldera collapse. (Lockwood and Lipman, 1987).

The evolution of Mokuaweoweo.

There is evidence of a low fault scarp on the south edge of the caldera which may be the buried rim of an older caldera. From about 1.5 - 0.75 ka, the summit area contained a lava lake which fed the northwest and southeast flanks (Lockwood and Lipman, 1987).

The youngest flows truncated by Mokuaweoweo are estimated by Lockwood and Lipman to be  $0.59 \pm 0.07$  ka and were probably erupted from fissures parallel to the present rim, as is evidenced by dikes in the northwest wall. The caldera formed around 0.75 ka, after which time surface flows were reduced. In 1794, the depth of Mokuaweoweo was recorded by Archibald Menzies to be "about 400 yards" deep. Subsequently, it continued to be filled by lava-lake activity. The inner pit first overflowed in 1914.

The 1984 eruption nearly completely covered the floor of Mokuaweoweo. These lavas are uniform, sparsely porphyritic tholeiitic basalt, with phenocrysts of forsteritic composition (Lockwood et al., 1987). Major element and X-ray fluorescence also show that the 1984 lava is generally uniform in composition, except for one flow off the SWRZ. This homogeneity is typical of most historical Mauna Loa lavas (Wright, 1971); currently most lavas erupted from the summit caldera, NERZ and upper SWRZ also preserve this pattern. In comparing 1984 lavas to the earlier erupted 1975 lava, Lockwood and others (1987) have concluded that the uniformity of the 1984 (less evolved) lavas suggests that they were derived from deeper reservoir.

### Observations

In the following paragraphs, I will present my observations of the Viking images of Olympus Mons and Ascræus Mons calderas and Mauna Loa's Mokuaweoweo caldera using air photos and TIMS images. The observations will be presented under the two categories of wrinkle ridges and lava flows. I will concentrate on Ascræus Mons in looking at flank flows since they were numerous and easily identified on this volcano compared to Olympus Mons. Concerning wrinkle ridges, I will concentrate on Olympus Mons, for the same reason.

## Lava Flows

On Ascræus Mons, the presence of lava flows (Figure 9) was much more obvious than on Olympus Mons. At the highest resolution (17 m/pixel, Figure 10), the flanks of Olympus Mons appeared to have a few lava flows, but the separate contacts were difficult to discern. Lobate flow fronts, source vents and lava tubes were not visible on the flanks or the caldera rim.

The sketch map of Mokuaweoweo (Figure 11) was produced using air photos (Figure 12) rather than TIMS images. Three distinct flow surfaces of varying color and texture were mappable, designated by the three different patterns on the sketch map. The sketch map was then compared to the TIMS image of Mokuaweoweo (image appears slightly distorted due to angle of instrument). Based on color alone, many more flow units are discernable. Consider the areas boxed off in Figure 13. Here we compare the areas labelled "g" and "y", which is correspondingly labelled on each map. The two are very distinctly different on the TIMS image (green/yellow transition), but on the sketch map, they are not distinguishable. The flow to the south (marked "s") which overflows out of North Pit into the main caldera appears dark on the air photo, and was mapped as an older a'a flow (stippled pattern). The yellow color on the TIMS image suggests that it is in fact the same flow as that of the caldera floor, perhaps from the 1975 flow. The prehistoric flows which appear white on the air photos and were mapped as unpatterned units have different spectral signatures. The dark green flow on the TIMS image is distinctly different from the turquoise blue to the south, even though these look texturally alike on the air photos.

In areas where pahoehoe flows turn into a'a flows as they travel down-slope and degas, the TIMS images were particularly useful in making out surface roughness (for example, areas marked "t"). Even in color air photos, the pahoehoe-a'a transition is

difficult to map without some field data. For example, in the flows which originated in the North Pit and flowed North (yellow), the color transition from yellow to pink represents the pahoehoe-a'a transition.

Flows on Ascræus Mons are quite common, and are much more mappable than on Olympus Mons. Figure 9 shows a high resolution image of the summit caldera with flows truncated by the rim and a lava channel. A sketch map (Figure 14) was produced of the flank of Ascræus Mons down-slope of the caldera rim, with most of the flows travelling southwest. The flows mapped ranged in length from 45 km to 2.25 km. The lava channels were also mappable due to their relief relative to the surrounding flows. The longest channel was 21 km and the shortest was 1.5 km. Most of the channels, regardless of their length, were sinuous in nature.

Difficulties were encountered in mapping separate flow units from the Viking images when the flow was not thick enough to produce an obvious flow front. As in Figure 9, features such as lava channels are quite distinct from the surrounding terrain. Although many lobate flow fronts and flow contacts are visible on the sketch map, the distinction between flow units and their identification as flank or fissure eruptions versus pre-caldera eruptions is difficult to determine. Further, the roughness of the surface was not easily recognized, making it almost impossible to identify a'a and pahoehoe flows or the point of the transition.

### Wrinkle Ridges

One of the most prominent features of the summit caldera of Olympus Mons is the presence of wrinkle ridges on the floor of the caldera. It was difficult to conclude with confidence if the ridges formed simultaneously, or if they represent several resurfacing events. The ridges are concentrated on the southwest portion of the caldera floor, where

three craters seem to overlap (Figure 15). Figure 16 is a sketch map of the area, showing grabens and occurrences of wrinkle ridges. The ridges appear to radiate from each of the different crater centers and are rarely concentric with the circumferential graben of the main caldera. The widths of the ridges vary from 0.1- 3.0 km in width (Mouginis-Mark, 1981), and vary in length from 0.5 km to 10 km in length in the area examined. Also present in Figure 15 is what has been interpreted as a vent (Mouginis-Mark, 1981). Lava flows on Olympus Mons were difficult to distinguish in the images studied.

The caldera floor of Mauna Loa also has wrinkle ridges present, although with somewhat of a different character. Using air photos, wrinkle ridges were observed, primarily along the floor of the main caldera (Figure 11, Figure 12), covered mainly by 1984 lava. The ridges on Mauna Loa averaged 215 m in length, with a maximum of 1.3 km and a minimum of 150 m. The orientation of the wrinkle ridges was concentric about the central rift zone of Mokuaweoweo. No wrinkle ridges were observed to be radial in nature, as was found on Olympus Mons. The ridges were found on both the 1975 and 1984 flows on the caldera floor.

Using the TIMS images of Mokuaweoweo (Figure 3), the wrinkle ridges were discernible, primarily after the decorrelation or principal component stretch (Figures 3b and 3c) had been applied to the data. It was easier to pick out ridges which were associated with different flows on the TIMS data, since these flows appeared as different colors. Although air photos were not available for the southwest portion of Mokuaweoweo, the ridges in this area were also obvious on TIMS data and were concentric about the central fissure as the smaller ones were (Figure 3). The graben around Mokuaweoweo also showed up distinctly in the TIMS, which suggests that for Olympus Mons and Ascræus Mons, if we had similar data, it would be easy to identify flows which originated from grabens or fissures.

### Interpretations

The above observations support the notion that multispectral data contains a wealth of information not currently available for planets other than Earth. TIMS data greatly facilitated mapping flows of Mokuaweoweo and surface texture was much more obvious than was on air photos. This kind of data helps to distinguish between flank and fissure eruptions, and the nature of these flows. Further, we can learn more about viscosity, volumetric flow rate, shear rate, and changes due to degassing by examining the pahoehoe-a'a transition (Rowland and Walker, 1990). Rowland and Walker have found that a'a, with a high volumetric flow rate ( $> 5-10 \text{ m}^3/\text{s}$ ) result from a rapid emptying of the magma chamber. Pahoehoe, with a lower volumetric flow rate ( $< 5-10 \text{ m}^3/\text{s}$ ) would probably come from a slower draining magma chamber deeper within the system which allows for loss of gasses.

In the case of Mauna Loa, information such as surface roughness and texture of flows may be obtainable from field studies. However, one great advantage seen in utilizing remote sensing data such as TIMS is that it offers uniform coverage of a large surface. Field work in remote or inaccessible areas does not always offer optimum field conditions, and human error is more likely to occur in collecting data over such a large area. Even with the aid of air photos, it is often difficult to distinguish individual flow characteristics due to subtle color differences. Since TIMS images are based on thermal properties, digital data which has been computer enhanced greatly facilitates making these distinctions.

Spectral data similar to TIMS would enable us to make great advances in the study of Martian volcanoes. Particularly for volcanoes such as Olympus Mons and Ascræus Mons, where we know that flows exist, but most data are inconclusive concerning the details of flow texture, length and origin. Structural features such as the circumferential

graben could be further investigated, obtaining information on flow origins. Although the analog on Mokuaweoweo is much smaller, we have seen how well these structures show up in TIMS.

The orientation of the wrinkle ridges relative to the main fissure of Mauna Loa suggest that they are in fact compressional features, associated with the withdrawal of magma from the underlying chamber. The erupted lava has been exposed long enough to form a crust without completely solidifying, and then withdraws back into the chamber through the fissures. Walker (1990) suggests that, in historic time, 30% of the lava erupted from Mokuaweoweo as been absorbed, and lava is then erupted as flank eruptions. Indeed, we see many flank eruptions on Mauna Loa, but data fro Martian volcanoes is inconclusive as of yet.

The nearly uniform composition of most of the floor of Mokuaweoweo, confirmed by uniform color on TIMS images, suggests that the ridges are thus compressional features on the caldera floor. On Olympus Mons, such data would be useful in determining the distribution of flows on the caldera floor, particularly in the area where wrinkle ridges are concentrated. It would be useful to know if the caldera floors have experienced one or more resurfacing events, and how different each flow is mineralogically between resurfacing events. Although flank eruptions are not obvious on Olympus Mons, wrinkle ridges suggest by analogy with Mauna Loa that flank eruptions should be present. Mougini-Mark and Zuber (1989) investigated the topography of the largest Olympus Mons caldera and noted that the wrinkle ridges occurred at the lowest portion of the caldera. This observation can place constraints on the magma chamber depth, which was calculated to be half the caldera radius, similar to that estimated for Hawaiian (Kilauea) volcanoes.



### Future Missions: Mars Observer and Sample Return Mission

The Mars Observer (MO) Mission, a project currently planned for a September 1992 launch, will provide us with many more details on the surface and atmosphere of Mars. Observations will be made over a period of one year, addressing such objectives as the global elemental and mineralogical character of the surface material, geophysical characteristics, nature of volatile material, and the structure of the atmosphere (Albaugh, 1991). The mission is expected to provide us with a more systematic global view of Mars.

There will be eight instruments on board the Mars Observer designed to accomplish the objectives. Two instruments which will fly on Mars Observer will combine two types of remote sensing used in this study. The Mars Observer Camera (MOC) is a line scan camera which will use both wide-angle and narrow-angle optics to produce a global data set of images with 7.5 km/pixel resolution, selective moderate resolution (480 m/pixel), and very selective high-resolution (1.4 m/pixel) images. MOC will hence provide a more uniform global view of the surface and enable atmospheric, meteorological and climatological studies to be performed. The Thermal Emission Spectrometer (TES) is a Michelson interferometer which will cover a spectral range of 6.25 to 50 micrometers. TES will allow us to determine and map the composition of the surface minerals, rock and ices. Further, we will be able to perform detailed studies on the composition, grain size and spatial distribution of the dust and clouds. Thermal inertial and albedo will also be measurable using TES, providing information on particle size of rocks.

Studies such as these show that data from TES will be extremely useful in unraveling more of the history of the Martian surface. We have already seen that TIMS data is extremely helpful in characterizing the nature of flows on the Mauna Loa, where it is often difficult to do field work due to high altitudes.

The Mars Sample Return Mission, which is still in the planning, could greatly utilize data obtained from MO in deciding on the most feasible landing site(s). Some of the major science questions being addressed by the sample return scientists are complex in nature: the origin of the SNC meteorites, accretion and core formation, chronology of formation of the atmosphere, calibration of cratering ages, and mantle mineralogy and composition. Precursor missions such as MO are essential in establishing with confidence the most appropriate areas to accomplish these objectives.

### Conclusions

Although remote sensing is still a relatively new tool in geology, we can look forward to many more applications as computers and instruments become more sophisticated. The main advantage of utilizing remote sensing in terrestrial studies is that it provides uniform coverage of large areas, in effect making it more efficient for mapping and determination of indistinct flow types. It should be emphasized that ideally, remote sensing data are most effective when examined in conjunction with other types of remote sensing data from different wavelengths, field studies, or air photos.

This study has confirmed that the character of Martian Volcanoes is much more complex than originally believed. Further studies need to begin analyzing Martian volcanoes in terms of other terrestrial analogs besides Hawaiian shield volcanoes, although this comparison may still be valid for certain volcanoes like Olympus Mons. Perhaps a classification system similar to that suggested by Crumpler and Aubele (1989) would be useful in facilitating further planetary studies. Future EOS and other precursor missions to Mars planned by NASA promise extensive data sets for terrestrial volcanoes such as those found in Italy, The Galapagos and Alaska. The mission of EOS volcanology project will

be to monitor volcanoes uniformly on a global scale, assessing hazards and aiding in eruption prediction.

The classification by Crumpler and Aubele (1989) suggests that Ascraeus Mons is more appropriately compared to Galapagos central volcanoes, West African Rift volcanoes, and Hekla volcano in Iceland, based on linear patterns in vent arrangements and a single fissure trend. Olympus Mons is more correctly classified with Hawaiian volcanoes with vents, fissures and rifts to follow pre-existing structural fabric orientations, changing as the volcano grows. We have confirmed the linear quality of the Ascraeus Mons, with one central linear trend running NE-SW and the absence of wrinkle ridges on the caldera floor. On Olympus Mons, the presence of wrinkle ridges on the caldera floor as on Mokuaweoweo suggests that there may be many tectonic stresses on the volcano as a result of magmatic inflation and deflation, buttressing effects, or interactions between local stress fields (Crumpler and Aubele, 1989).

Our knowledge of the solar system and other planets is almost completely derived from remote sensing information. For the majority of the planetary environments, this will be the only way we can study these bodies. Beginning with early observations of Brahe and Kepler, Mars scientists have been utilizing progressively more sophisticated data sets. While we have not completely exhausted the limits of the Mariner and Viking Mission data, our curiosity has been further probed, and future missions offer even more exciting discoveries. The applications of this technology to terrestrial studies is equally as exciting, since it will for once offer a uniform data set upon which scientist can begin monitoring volcanic activity.

References Cited

- Abrams, M., Abbott, E., and Kahle, A., Combined use of visible, reflected infrared and thermal infrared images for mapping Hawaiian lava flows, *J. Geophys. Res.* 96, B1, 475-484, 1991.
- Albaugh, D.H. (Ed.), *The Mars Observer*, JPL 410-30 issue 2, Pasadena, California, 1991.
- Arvidson, R. E., Goettel, K. A., and Hohenberg, C. M., A post-Viking view of the geologic evolution of Mars, *Res. Geophys. Space Phys* 18, 565-603, 1980.
- Basaltic Volcanism Study Project, *Basaltic Volcanism on the Terrestrial Planets*, Pergamon Press Inc., New York, New York, 1981.
- Blasius, K. R., Topography of six martian volcanoes from high-altitude systematic stereo imaging of Viking orbiter 1, *Bull Am. Astron. Soc.* 11 : 573, 1979.
- Carr, M.H. (Ed.) *The Geology of the Terrestrial Planets*, NASA SP-469, US Govt. Printing Office, Washington, D.C., 1984.
- Carr, M.H., *The Surface of Mars*, Yale University Press, New Haven, Connecticut, 1981.
- Cox, A., and Hart, R. B., *Plate Tectonics: How it works*, Blackwell Scientific Publications, Inc., Boston, Massachusetts, 1986.
- Crumpler, L.S. and Aubele, J.C., Influence of Tectonic and Volcanic Stresses on the Flank Structure of Martian Volcanoes, *LPI Tech Report 89-06*, 25-27, 1989.
- Crumpler, L.S., and Aubele, J.C., Structural evolution of Arsia Mons, Pavonis Mons, and Ascraeus Mons: Tharsis regions of Mars, *Icarus* 34, 496-511, 1978.
- Greeley, R. and Carr, M.H., Volcanic Features of Hawaii: A Basis For Comparison With Mars, NASA SP-403, US Government Printing Office, Washington, D.C., 1980.
- Greeley, R., and Spudis, P.D., Ridges in western Columbia Plateau, Washington-analogs to mare-type ridges, *Lunar Planet. Sci. Abs.* IX, 411-412, 1978.
- Greeley, R. and Spudis, P.D., Volcanism on Mars, *Revs. Geophys. Space Phys.* 19, 13-41, 1981.
- Kahle, A.B., Gillespie, A.R., Abbott, E. A., Abrams, M.J., Walker, R.E, Hoover, G., and Lockwood, J.P., Relative dating of Hawaiian lava flows using multispectral thermal infrared images: a new tool for geologic mapping of young volcanic terranes, *J. Geophys. Res.* 93, B12, 15239-15251, 1988.
- Lillesand, T., and Kiefer, R., *Remote Sensing and Image Interpretation, 2nd ed.*, J. Wiley and Sons, Inc., New York, New York, 1987.

- Lockwood, J.P., and Lipman, P.W., Holocene eruptive history of Mauna Loa Volcano in *Volcanism in Hawaii*, USGS Professional Paper 1350, 509-535, 1987.
- Lucchita, B.K. and Klockenbrink, J.L., Ridges and scarps in the equatorial belt of Mars, *Moon Planets 24*, 415-429, 1981.
- Macdonald, G.A., Abbott, A.T. and Peterson, F.L., *Volcanoes in the Sea, 2nd ed.*, University of Hawaii Press, Honolulu, Hawaii, 1983
- Mouginis-Mark, P.J., Late-stage summit activity of martian shield volcanoes, *Proc. Lunar Planet. Sci. 12B*, 1431-1447, 1981.
- Mouginis-Mark, P.J., Sharpton, V.L., and Hawke, B.R., Shiaparelli basin, Mars: Morphology, tectonics and infilling history, *Proc. Lunar and Planet. Sci. 12A*, 155-172, 1981.
- Mouginis-Mark, P.J. and Zuber, M.T., The depth of Olympus Mons magma chamber as determined from the spatial distribution of tectonic features, *LPI Tech Report 89-06*, 74-75, 1989.
- Mutch, T. A., Arvidson, R.E., Head, J.W., Jones, K.L., and Saunders, R.S., *The Geology of Mars*, Princeton University Press, Princeton, New Jersey, 1976.
- NASA SP-441, *Viking Mission to Mars*, US Govt. Printing Office, Washington, DC., 1980.
- Rowland, S.K., and Walker, G.P.L., Pahoehoe and a'a in Hawaii: volumetric flow rate controls the lava structure, *Bull Volcanol 52*: 615-628, 1990.
- Siegall, B.S., and Gillespie, A.R. (Eds.), *Remote Sensing in Geology*, John Wiley and Sons, New York, New York, 1980.
- Stearns, H.T., *Geology of the State of Hawaii, 2nd ed.*, Pacific Books, Palo Alto, California, 1985.
- Strom, R.G. Lunar mare ridges, rings, and volcanic ring complexes. From *The Moon, Symposium 47 of the I. A. U.* , 187-215, Reidel, Dordrecht, Netherlands, 1972.
- Thomas, P.J., Squyres, S.W. and Carr, M.H., Flank Tectonics of Martian Volcanoes, *LPI Tech Report 89-06*, 60-62, 1989
- Walker, G.P., Geology and Volcanology of the Hawaiian Islands, *Pacific Science 44*, 4, 315-347, 1990.
- Watters, T.R., Wrinkle Ridge Assemblages on the Terrestrial Planets, *J. Geophys. Res.* 93, B9, 10236-10254, 1988.
- Wright, T.L., Chemistry of Kilauea and Mauna Loa lavas in space and time, *USGS Professional Paper 735*, p. 1-45, 1971.

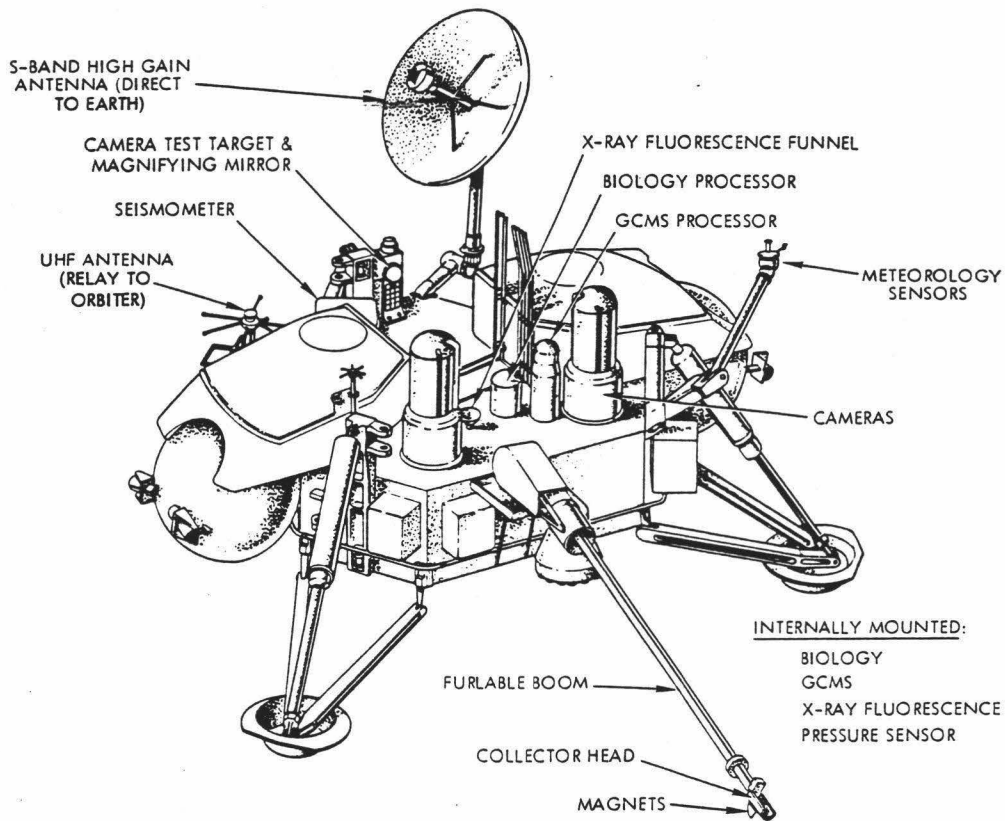


Figure 1 The Viking Orbiter, with vidicon (From Carr, 1981).

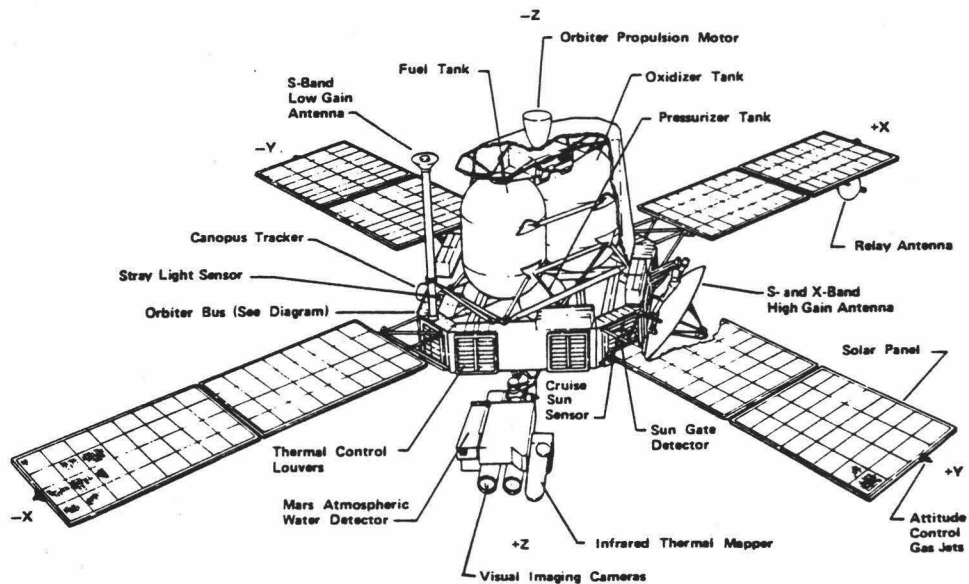


Figure 2 The Viking lander, with location of instruments (From Carr, 1981).

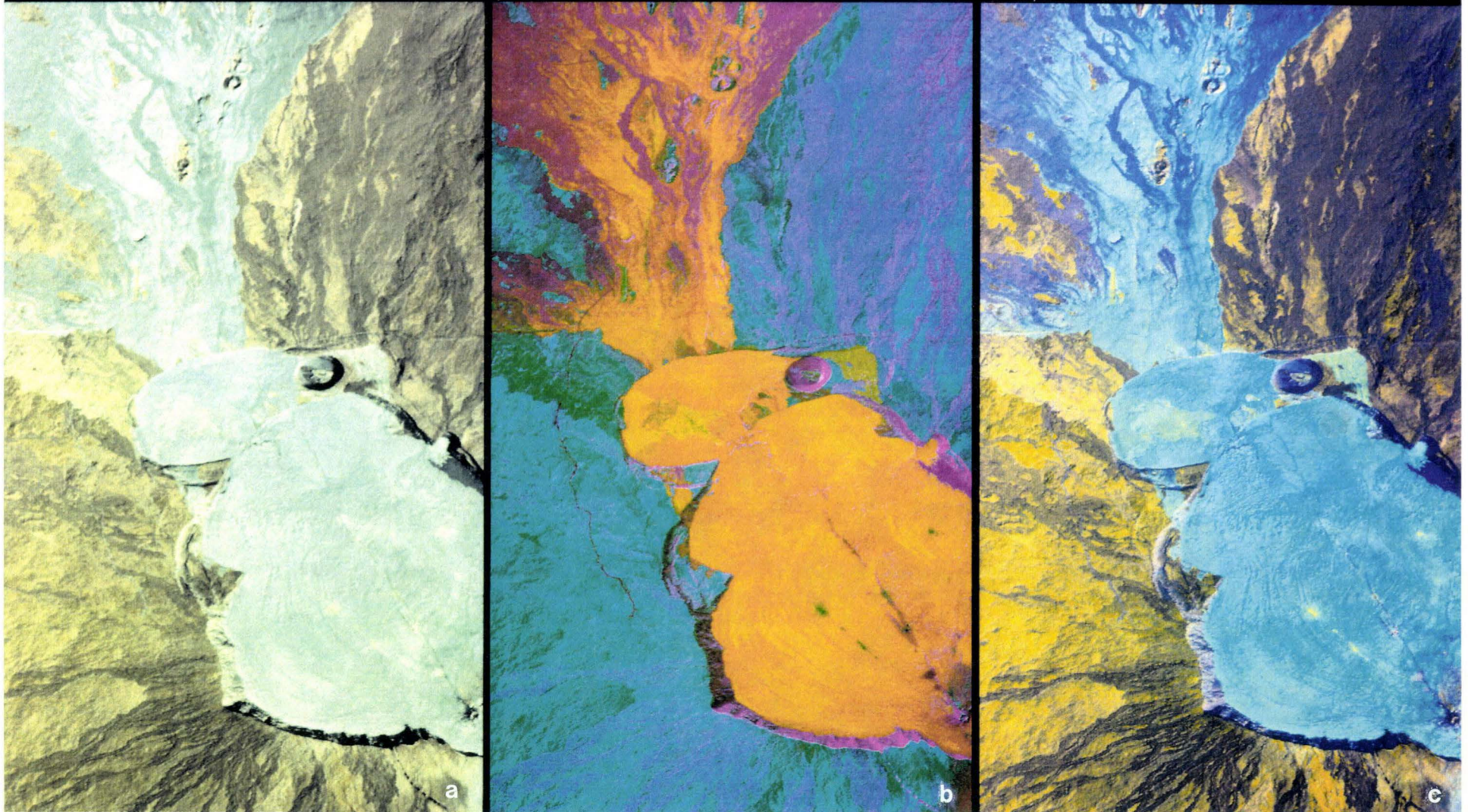


Figure 3 TIMS images used in this study. a) bands 6,1,3 b) principle components stretch of bands 2,3,1 c) decorrelatin stretch of bands 6,1,3.

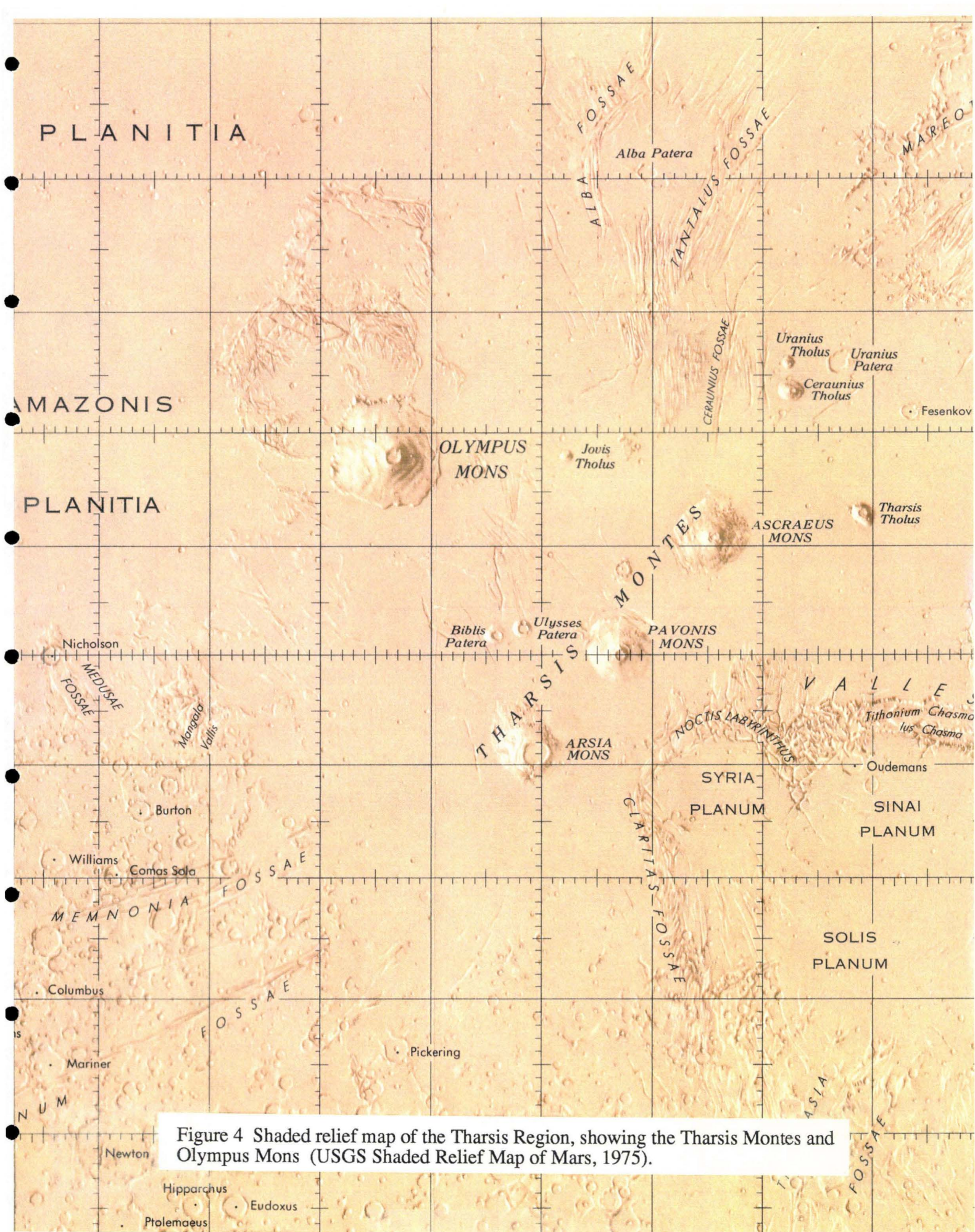


Figure 4 Shaded relief map of the Tharsis Region, showing the Tharsis Montes and Olympus Mons (USGS Shaded Relief Map of Mars, 1975).



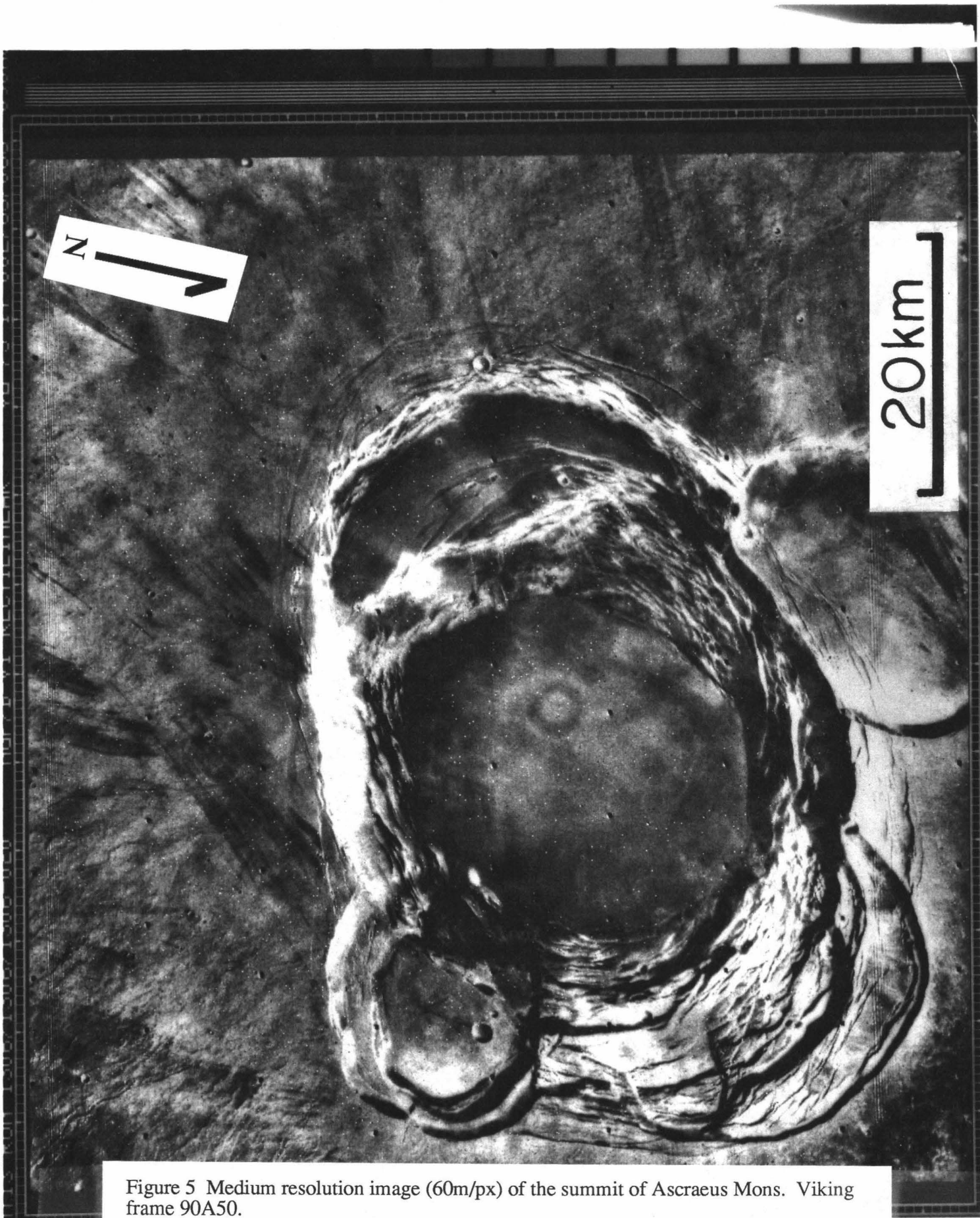


Figure 5 Medium resolution image (60m/px) of the summit of Ascreaus Mons. Viking frame 90A50.

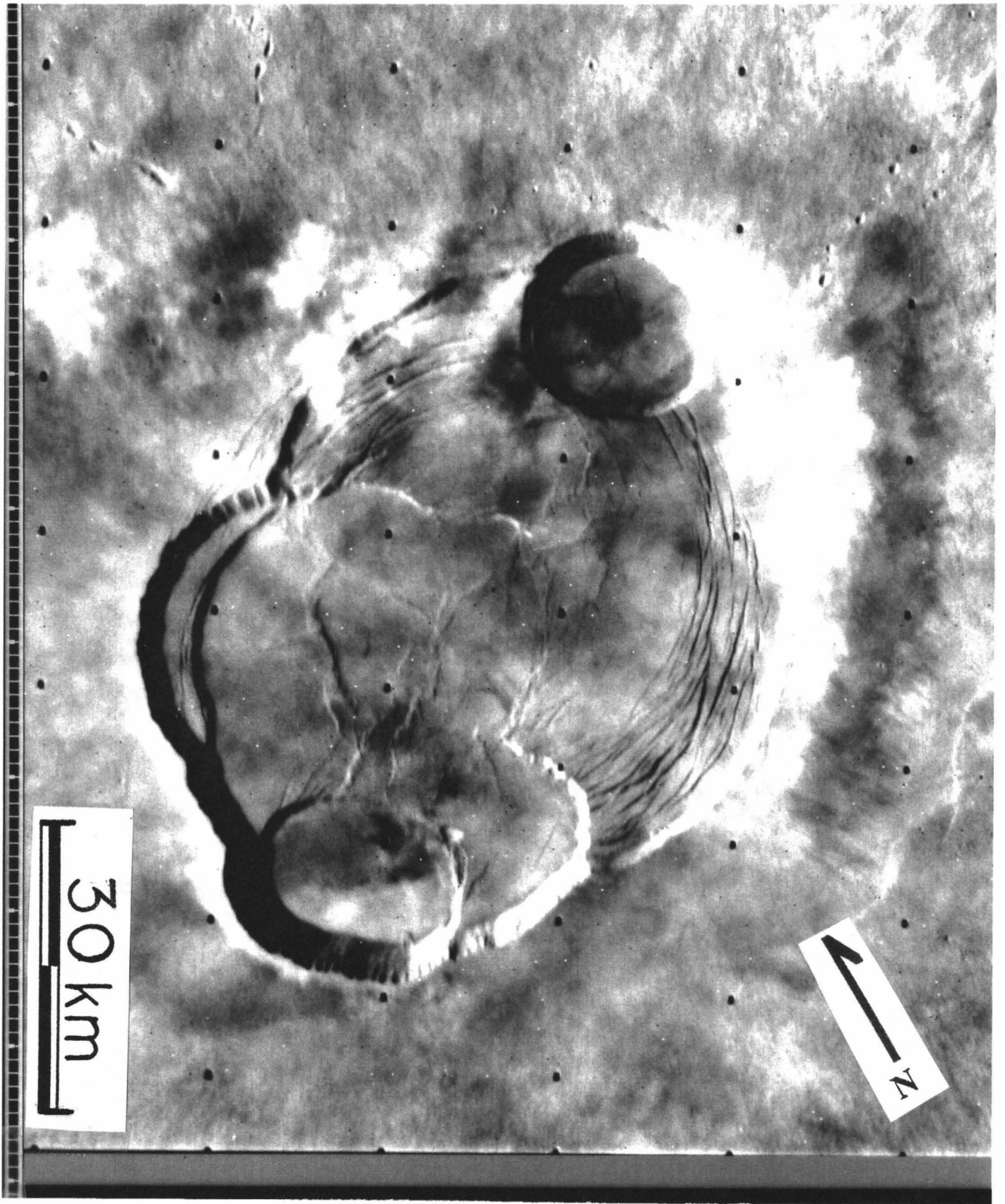


Figure 6 Medium resolution image (140 m/px) of the summit of Olympus Mons. Viking frame 46B31.

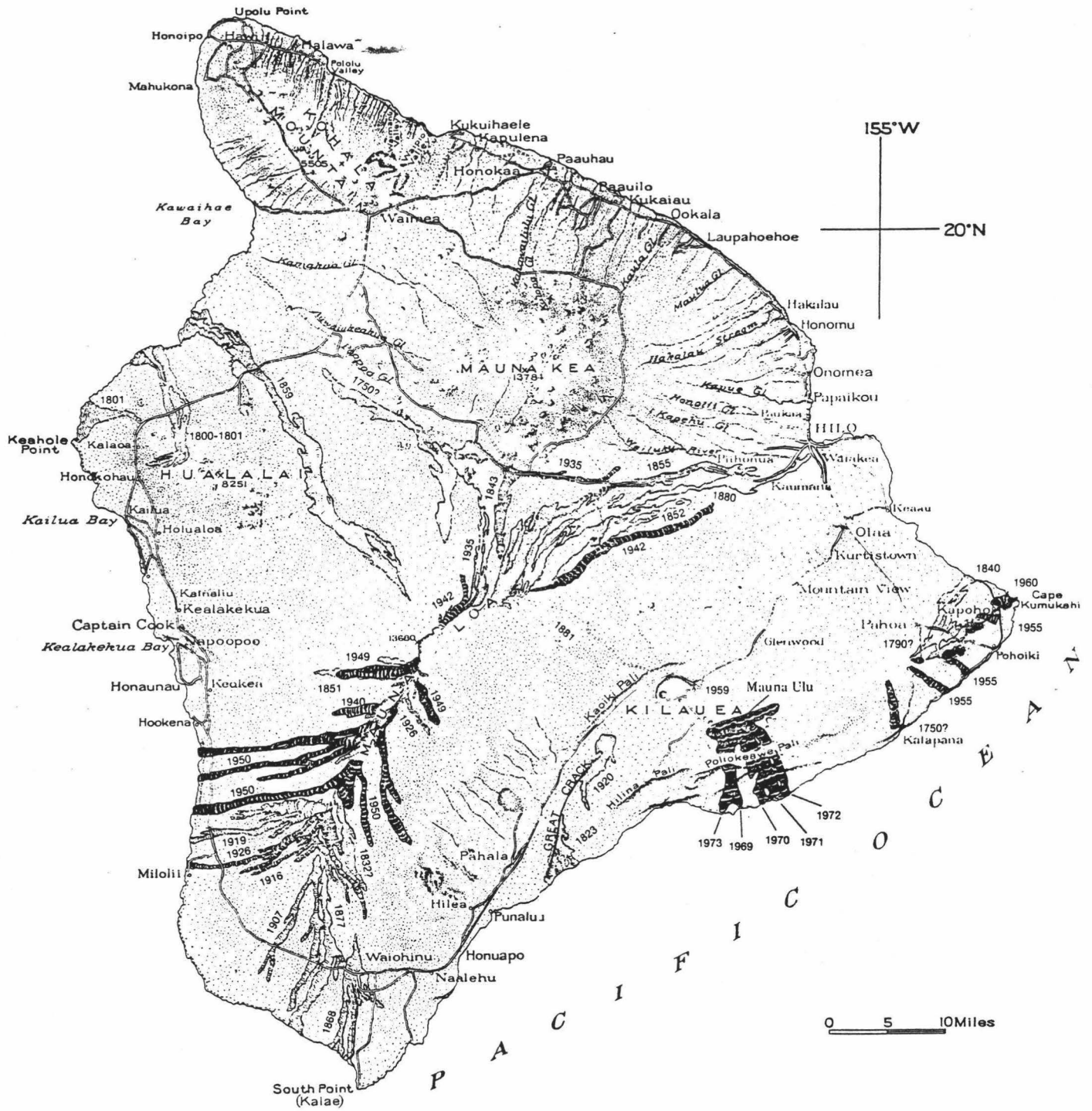


Figure 7 The Big Island of Hawaii, showing the five major volcanoes and historic lava flows to 1969 (After Macdonald and Abbott, 1970).

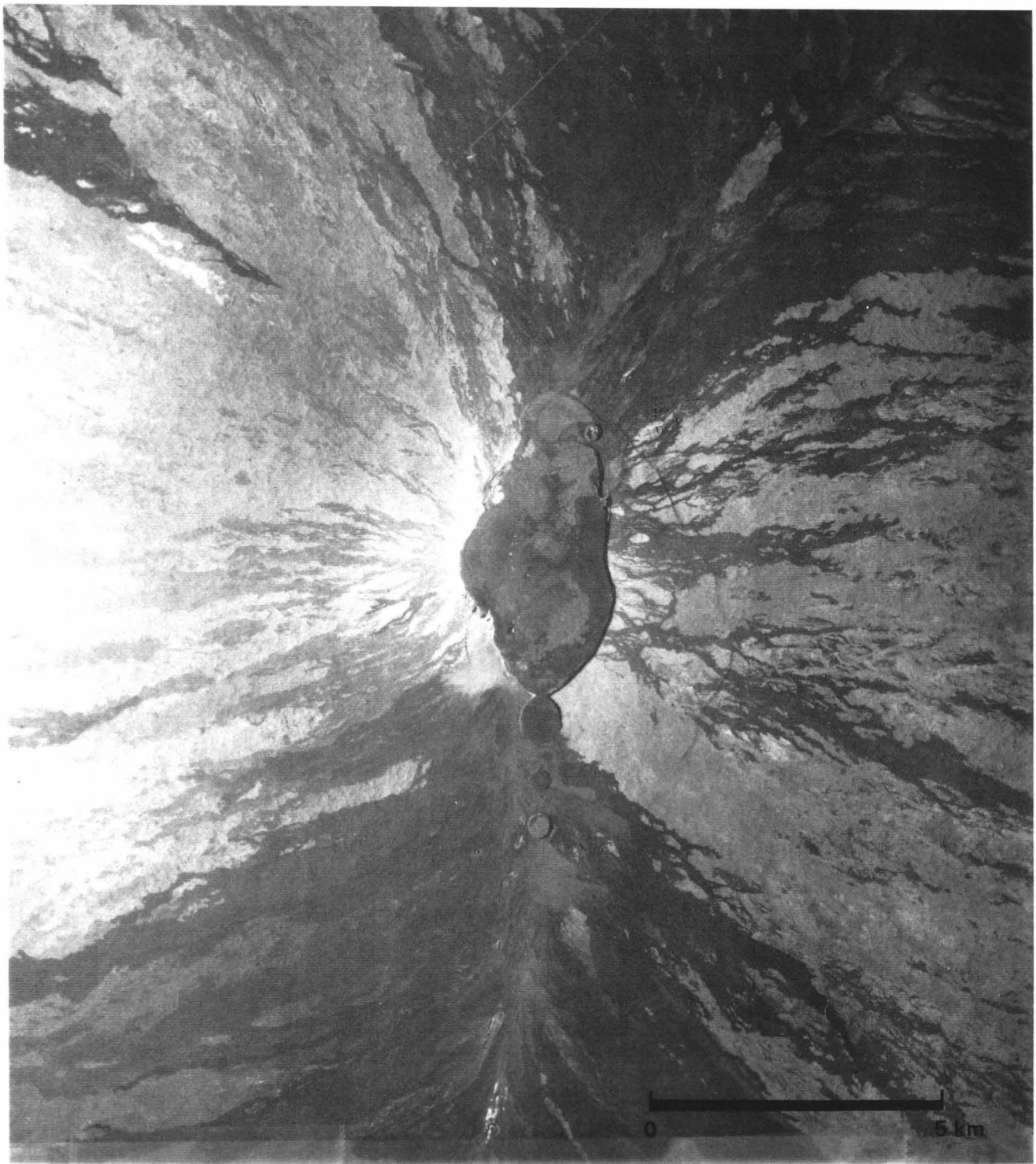


Figure 8 Air photograph of the summit of Mauna Loa, with North Pit, Lua Paholo, and the main caldera Mokuaweoweo. The darkest flows are from the 1949 eruption. (NASA-Amers U-2 high-altitude photograph, October, 1974. From Carr and Greeley, 1980).



MTIS RUN 9960/9960/2545-042

NGF/B-V1 RECTILINEAR

VO-75 2Y-0054423249

401B18

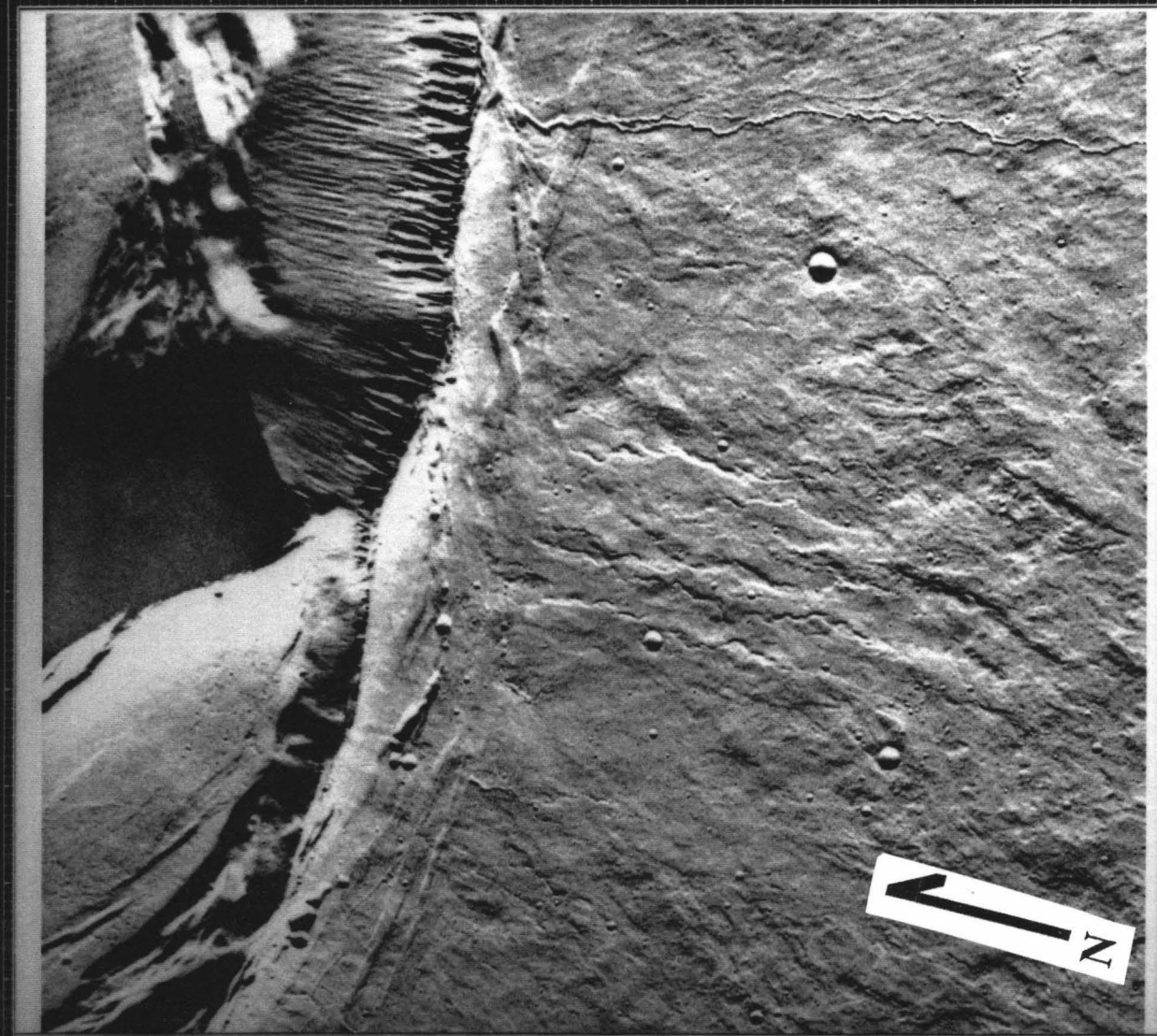


Figure 9 High resolution image of the rim of Asraeus Mons caldera. Note that flows are truncated by the formation of the crater. Sinuous feature is a lava channel. Viking frame 401B18.

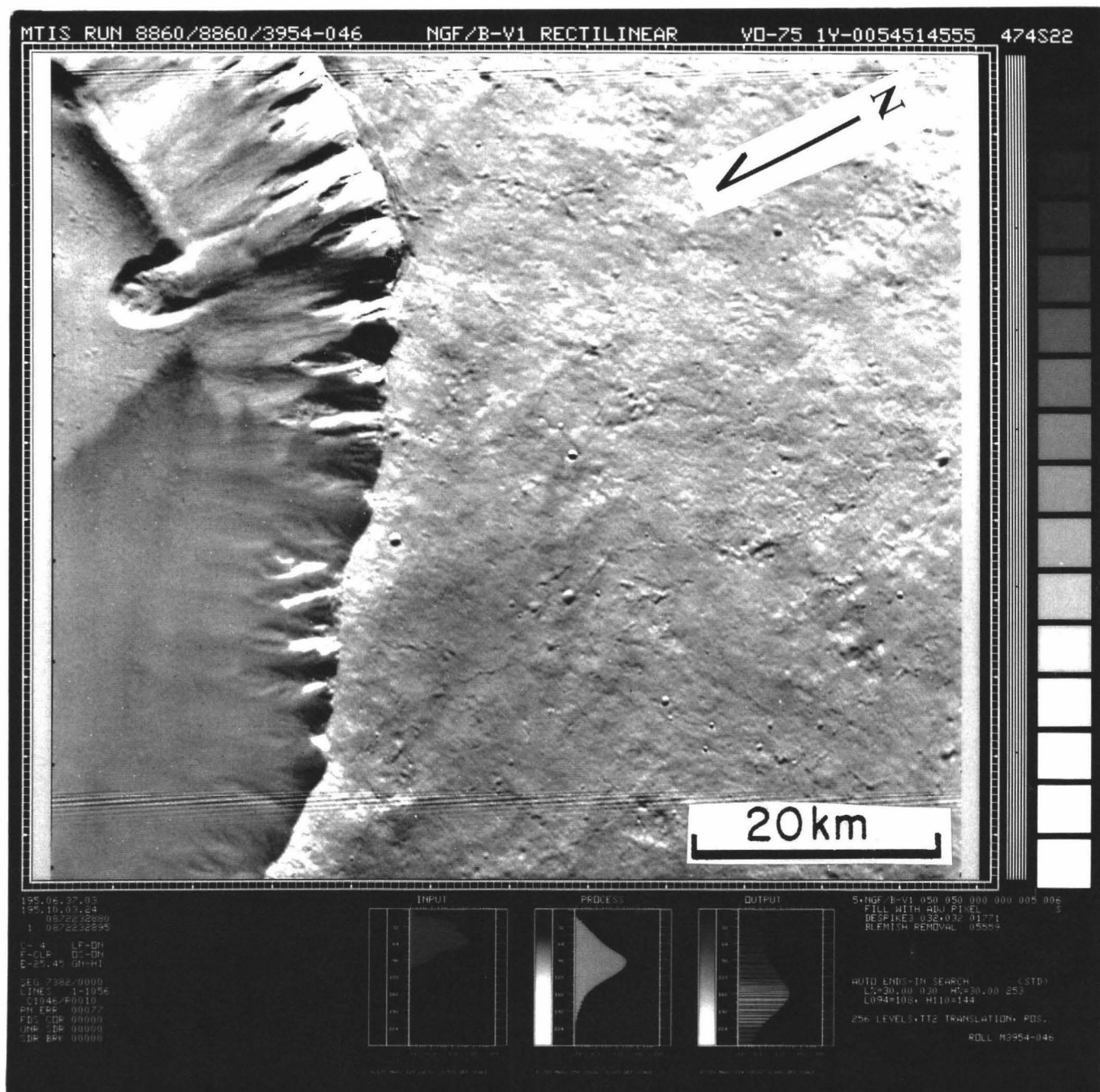
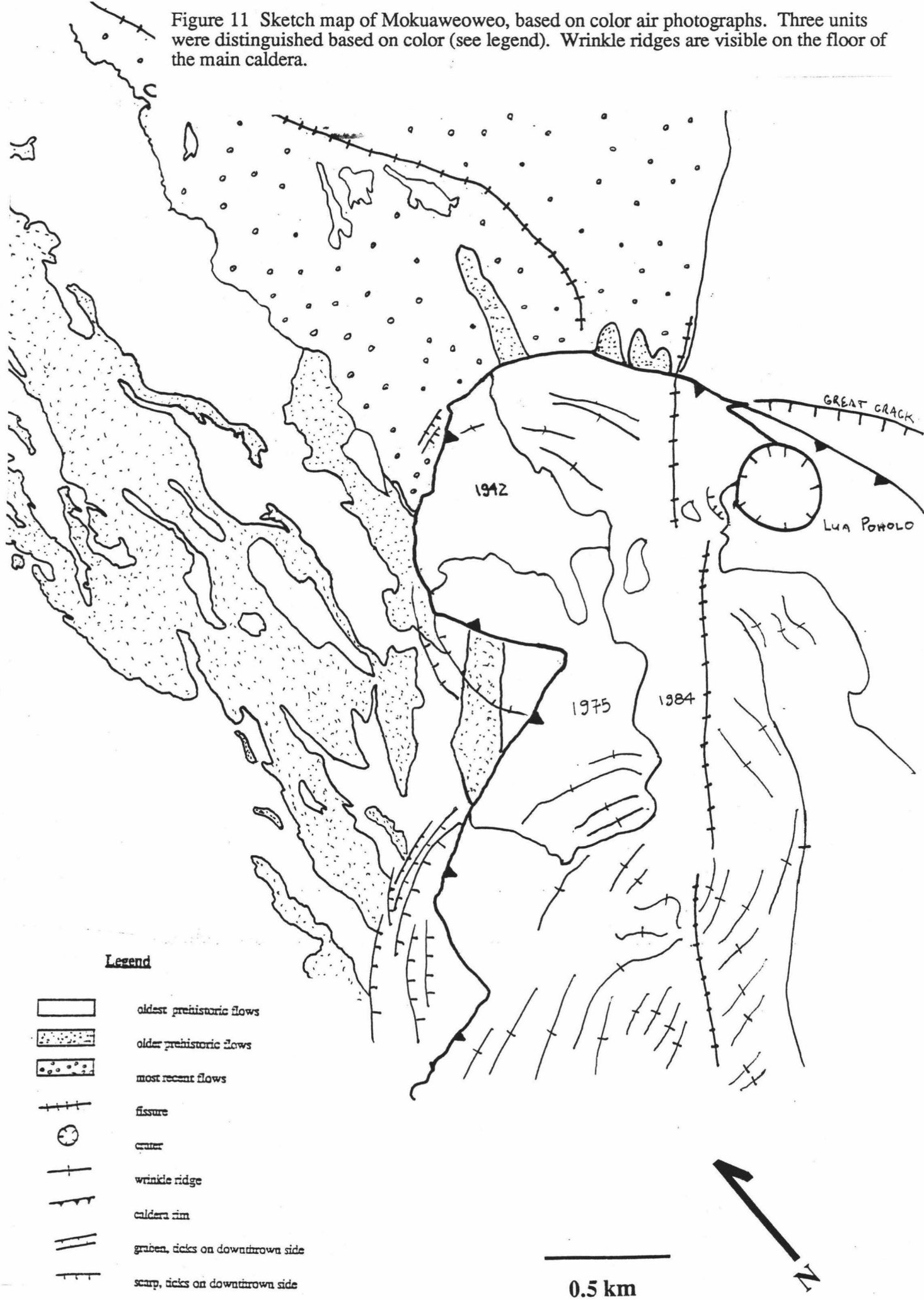


Figure 10 High resolution image of the caldera rim of Olympus Mons. Note how difficult it is to pick out separate flows on the flank. Feature on the north rim has been interpreted as a small landslide. Viking Survey 474S22.

Figure 11 Sketch map of Mokuaweoweo, based on color air photographs. Three units were distinguished based on color (see legend). Wrinkle ridges are visible on the floor of the main caldera.



03541

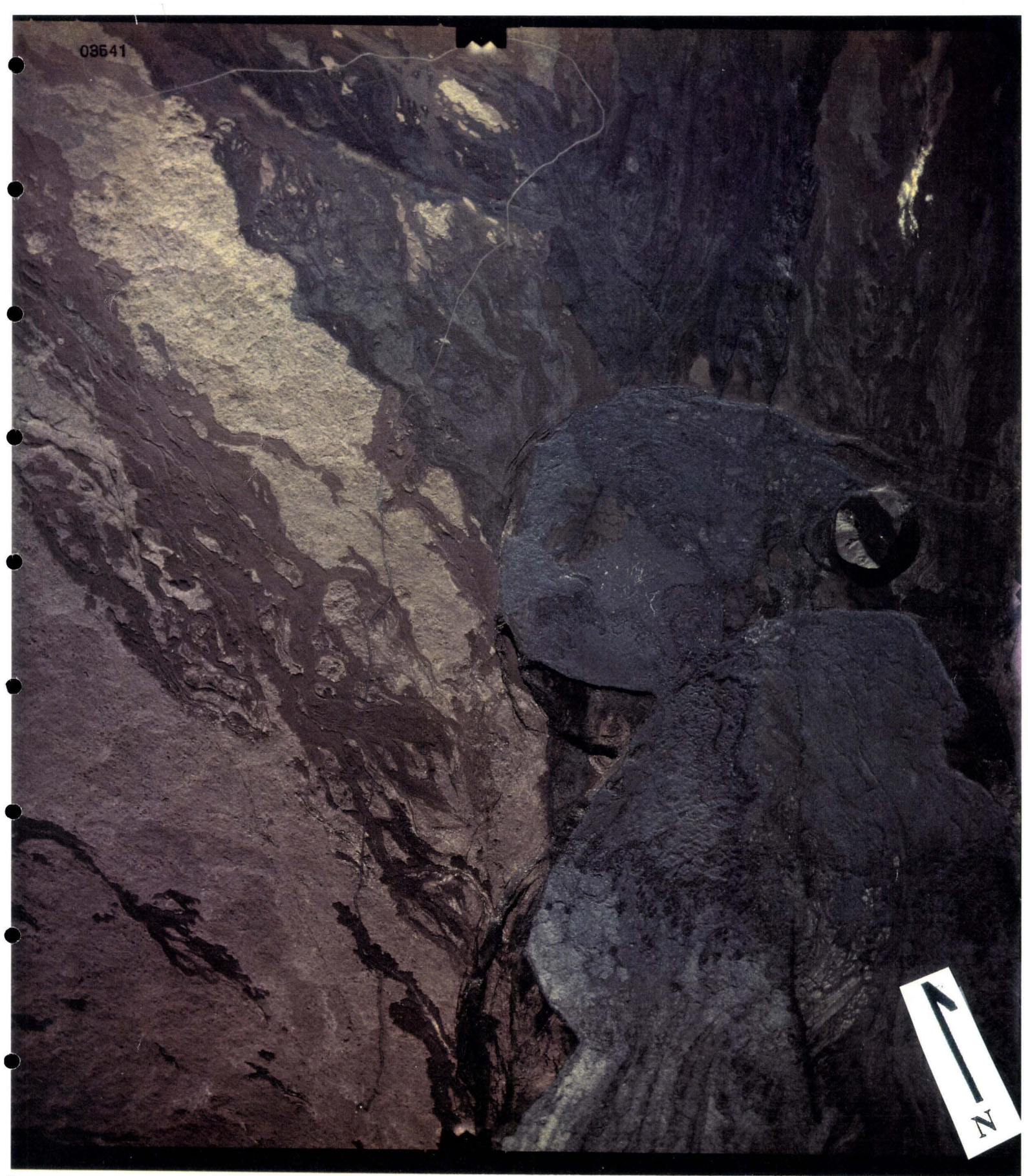


Figure 12 Air photograph used in producing sketch map of Mokuaweoweo (fig 11). Note the three different units and wrinkle ridges on the caldera floor.



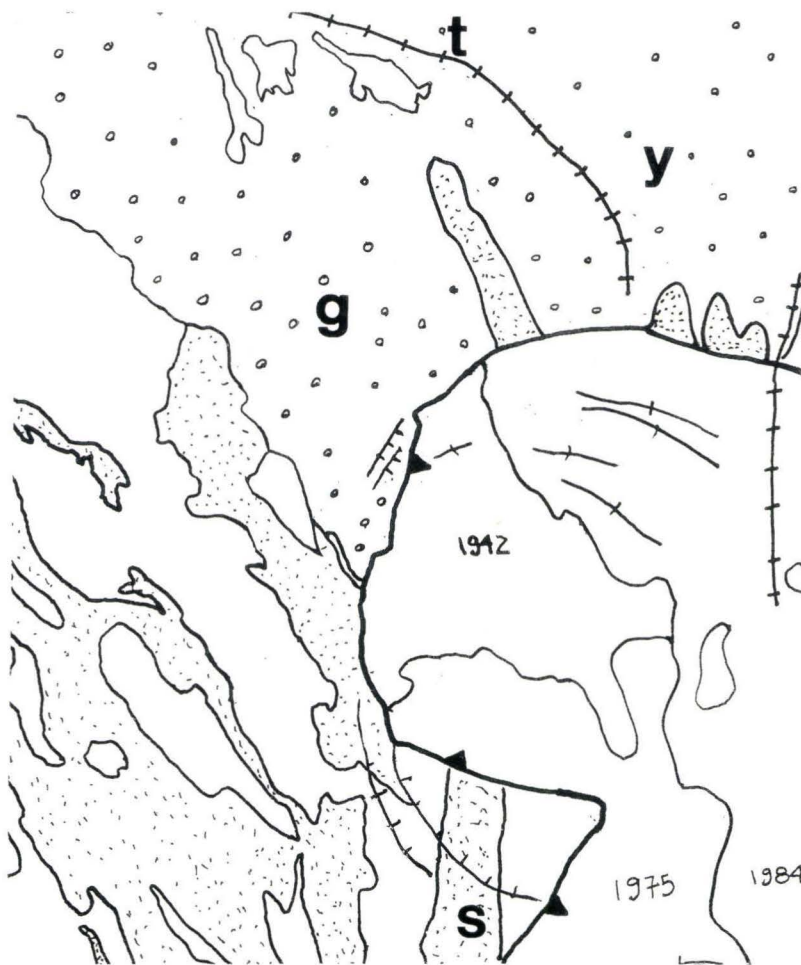
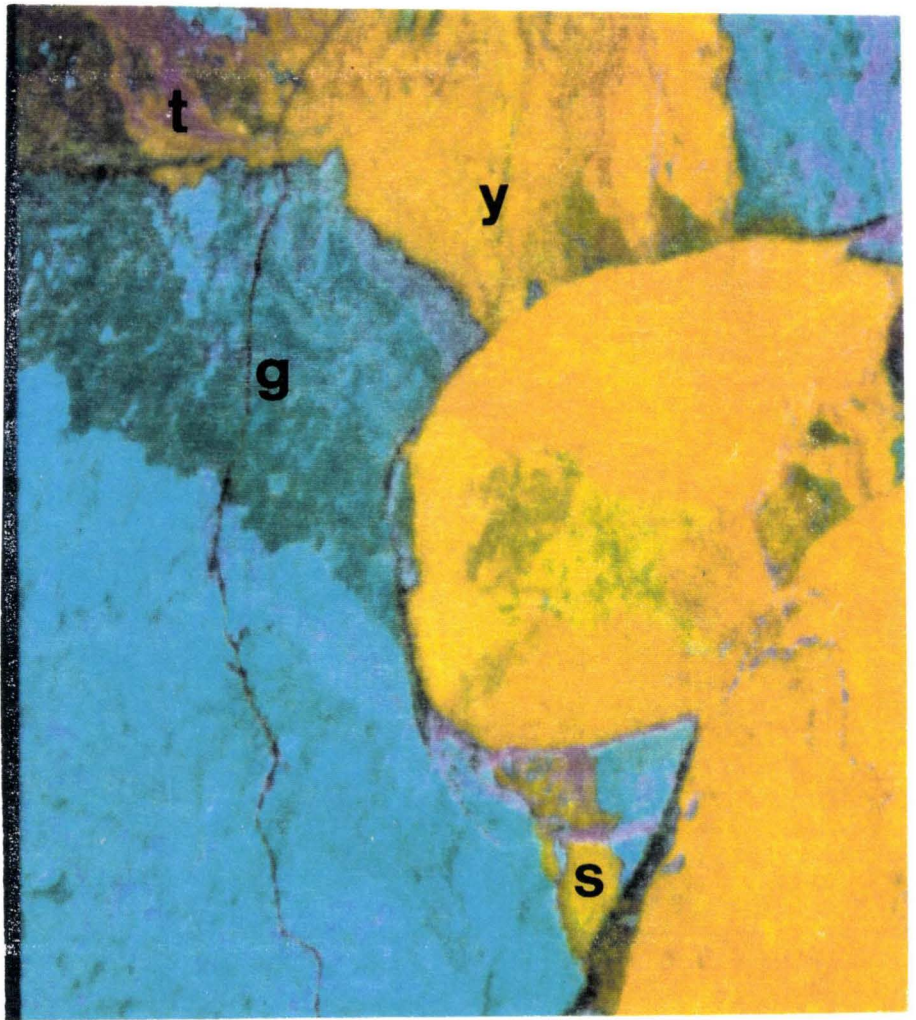


Figure 13 TMS image and sketch map comparison. The two areas are roughly the same, portion of northern caldera of Mauna Loa. Matching letters correspond to the same areas on either map.



approx. 0.5 km

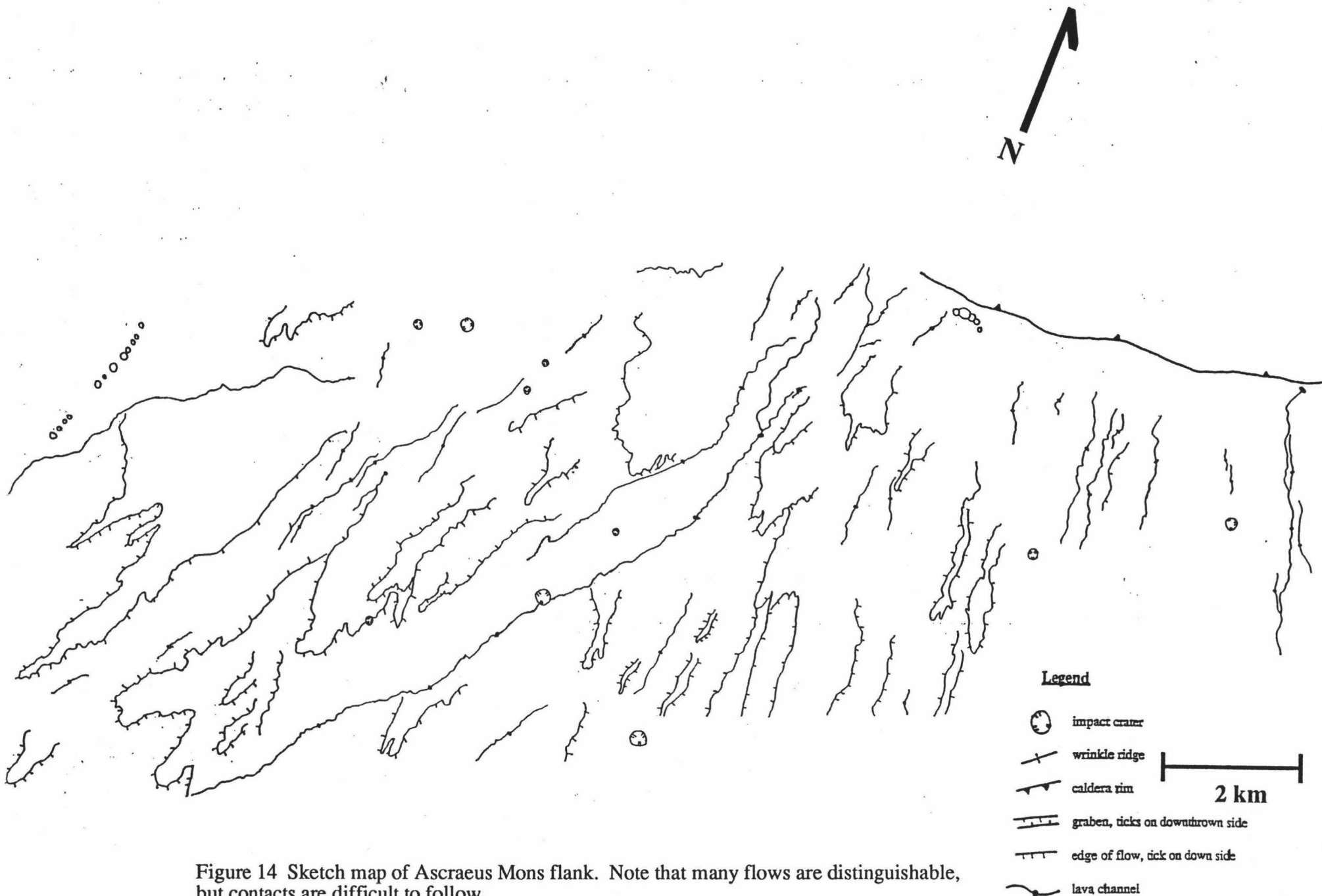









Figure 14 Sketch map of Asraeus Mons flank. Note that many flows are distinguishable, but contacts are difficult to follow.

**Legend**

-  impact crater
  -  wrinkle ridge
  -  caldera rim
  -  graben, ticks on downthrown side
  -  edge of flow, tick on down side
  -  lava channel
-   
**2 km**

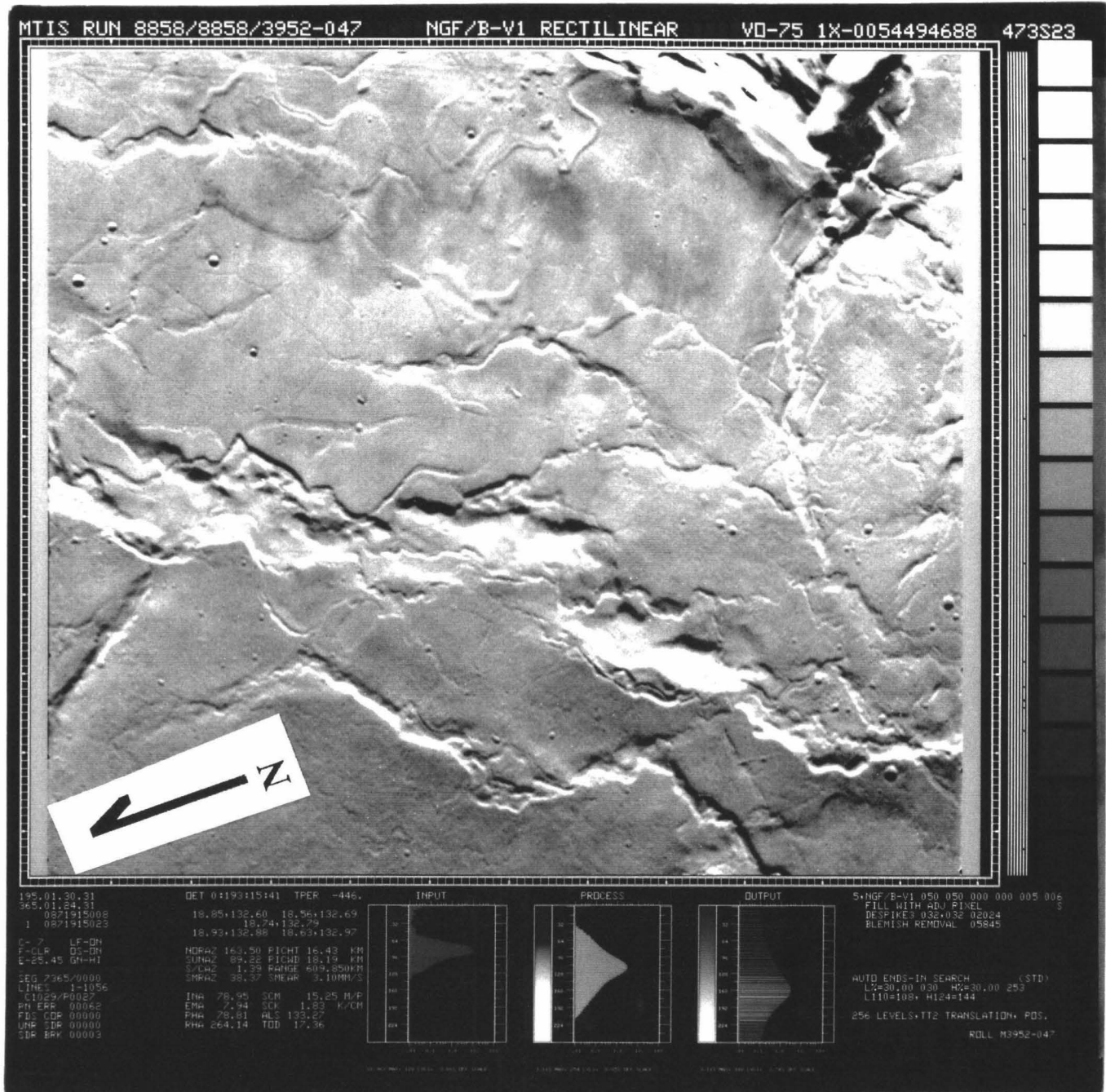


Figure 15 High resolution image (15 m/px) of the floor of Olympus Mons caldera, showing wrinkle ridges in detail. Viking image 473S23.

